AD-A070 454 ARMY ARMAMENT RESEARCH AND DEVELOPMENT COMMAND DOVER--ETC F/G 20/12
THE RESPONSE OF GERMANIUM TO LARGE AMPLITUDE SHOCK WAVES. (U)
JUN 79 P HARRIS

UNCLASSIFIED ARLCD-TR-79016 SBIE-AD-E400 317 NL

| OF |
AD
A070454

END
DATE
FILMED
7-79
DDC

(12) LEVEL II

AD

AD-E400 317

TECHNICAL REPORT ARLCD-TR-79016

THE RESPONSE OF GERMANIUM TO LARGE AMPLITUDE SHOCK WAVES

PAUL HARRIS

JUNE 1979

US ARMY ARMAMENT RESEARCH AND DEVELOPMENT COMMAND
LARGE CALIBER
WEAPON SYSTEMS LABORATORY
DOVER, NEW JERSEY

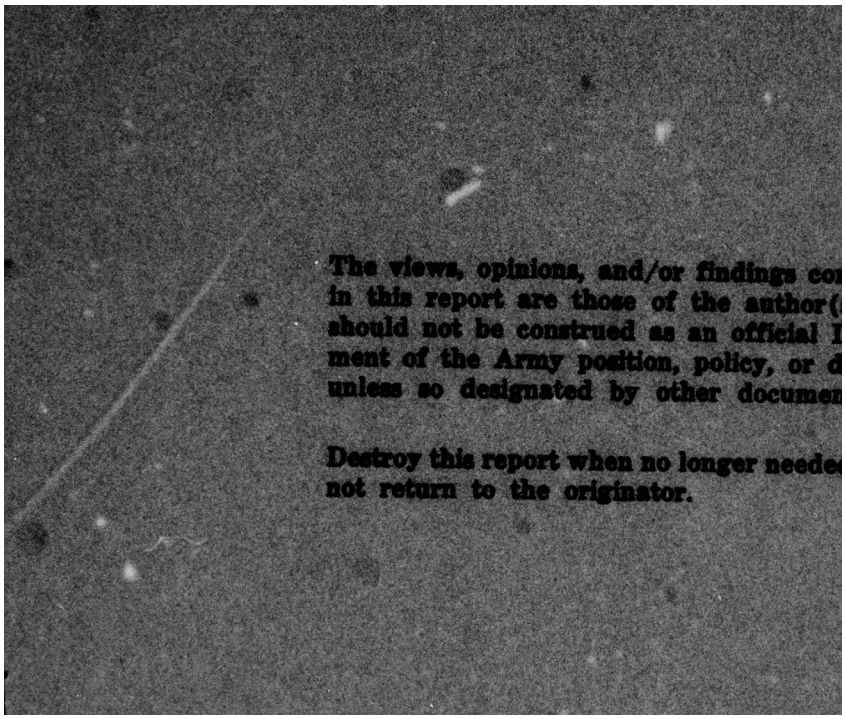
The views, opinions, and/or findings co
in this report are those of the author(
should not be construed as an official
ment of the Army position, policy, or d
unless so designated by other documen
Destroy this report when no longer neede
not return to the originator.

UNCLASSIFIED

SECURITY CLASSIFICATION OF THIS PAGE (When Data Entered)

REPORT DOCUMENTATION PAGE		READ INSTRUCTIONS BEFORE COMPLETING FORM
1. REPORT NUMBER Technical Report ARLCD-TR-79016	2. GOVT ACCESSION NO.	3. RECIPIENT'S CATALOG NUMBER
4. TITLE (and Subtitle) THE RESPONSE OF GERMANIUM TO LARGE AMPLITUDE SHOCK WAVES		5. TYPE OF REPORT & PERIOD COVERED 6. PERFORMING ORG. REPORT NUMBER
7. AUTHOR(s) Paul Harris		8. CONTRACT OR GRANT NUMBER(s)
9. PERFORMING ORGANIZATION NAME AND ADDRESS Commander U.S. Army ARRADCOM, ATTN: DRDAR-LCN Dover, NJ 07801		10. PROGRAM ELEMENT, PROJECT, TASK AREA & WORK UNIT NUMBERS
11. CONTROLLING OFFICE NAME AND ADDRESS Commander U.S. Army ARRADCOM, ATTN: DRDAR-TSS Dover, NJ 07801		12. REPORT DATE June 1979 13. NUMBER OF PAGES 36
14. MONITORING AGENCY NAME & ADDRESS(if different from Controlling Office)		15. SECURITY CLASS. (of this report) Unclassified 15a. DECLASSIFICATION/DOWNGRADING SCHEDULE

16. DISTRIBUTION STATEMENT (of this Report)

Approved for public release; distribution unlimited.

17. DISTRIBUTION STATEMENT (of the abstract entered in Block 20, if different from Report)

18. SUPPLEMENTARY NOTES

19. KEY WORDS (Continue on reverse side if necessary and identify by block number)

Shock waves in germanium
Semiconductor-to-metal transition
Brittle yielding
Ductile yielding
Band gap collapse

20. ABSTRACT (Continue on reverse side if necessary and identify by block number)

A tentative explanation for the first two (50 kb and 120 kb) experimentally observed shock wave transitions in single crystal germanium is presented. Calculations are carried out which suggest that the 120 kb transition is associated with the ductile yielding upon collapse of the conduction band onto the valence band (i.e., a semiconductor-metal transition without an associated transformation of the crystal structure). Arguments are also given which lead to the identification of the 50 kb transition as a brittle fracture phenomenon.

DD FORM 1 JAN 73 1473 EDITION OF 1 NOV 65 IS OBSOLETE

UNCLASSIFIED

SECURITY CLASSIFICATION OF THIS PAGE (When Data Entered)

ACKNOWLEDGMENTS

The author gratefully acknowledges relevant and helpful discussions with the following: Dr. R.A. Graham of Sandia Laboratories, Dr. W. H. Gust of Lawrence Livermore Laboratories, Dr. A. Jayaramar of Bell Telephone Laboratories, and Dr. A.K. Nedoluha of the United States Army Research and Standardization Group (Europe).

TABLE OF CONTENTS

TABLE

FIGURES

INTRODUCTION

The response of germanium to shock waves should be a theoretician's delight. Because of its extreme importance to the electronics industry, germanium (Ge) has probably been studied more than any other solid material. Its basic (i.e., infinitesimal disturbance) electrical, mechanical, and thermal properties are well understood in terms of the modern microscopic concepts of solid state physics. Many mechanical (as well as electromechanical) shock wave observations, however, have not yet been adequately explained.

In this report some of the well known infinitesimal disturbance properties of Ge are applied to shock wave observations. Calculations are presented which strongly hint that electronic band structure effects play a dominant role in at least one (the approximately 120 kilobars) dynamic pressure-volume derivative discontinuity observation. If the interpretation of the calculations is correct, a new view immediately develops for the Hugoniot elastic limit and the onset of ductility (metallic plasticity) in a single crystal semiconductor. That new view is correlated with the semiconductor-to-metal transition observations which are characteristic of the diamond structure.

Although silicon exhibits shock wave properties very similar to Ge, silicon (Si) is not treated in this report; more calculations need to be carried out before the Si results can be presented.

The calculations presented contain detailed band structure mathematics. Because this type of mathematics is not a common tool of shock wave physics, mini-summaries are presented (clearly set off from the main text) which allow the non-mathematically inclined reader to appreciate the significance of the calculations.

EXPERIMENTAL DATA

Gust and Royce have presented a complete orientational set of pressure-volume curves for Ge to approximately 200 kilobars. They report lower stress "transitions" occurring at approximately 50 kb and approximately 120 kb. Their data, while containing approximately 15 kb of scatter, are reproduced in table 1. The data are for a uniaxial strain shock propagating parallel to the indicated crystallographic directions.

Table 1. Lower stress shock transitions in germanium[a].

	Uniaxial Strain Direction <100>	<110>	<111>
First transition	58 kb	48 kb	47 kb
Second transition	117	119	125

[a] From W.H. Gust and E.B. Royce, J. Appl. Phys. 43, 4437 (1972).

The common[1,3] interpretation of the above transitions has been to identify the first transition as the Hugoniot elastic limit (HEL), and to identify the second transition as the semiconductor-metal (polymorphic) structural phase transformation as reported by Bundy[4]. Jacquesson and coworkers[5], while reporting essentially the table 1 data for the <100> and <111> directions, also report a third transition near 130 kb. Additionally, Jacquesson, et al[5], have shown some hesitancy to identify the various transitions.

This report tentatively identifies the first transition as a mechanical transition associated with brittle fracture, and the second transition as ductile (metallic) yielding. The third transition observed by Jacquesson, et al[5], may then turn out to be the structural phase transition observed (hydrostatically) by Bundy[4].

Before commencing with the electronic band structure details, it is worth noting that room temperature monocrystalline Ge only undergoes brittle fracture[6,7,8]. While twinning[8] may occur in room temperature Ge, that ductile twinning is always associated with stress concentration at a crack tip. The point is that the first yielding expected to be observed at room temperature under shock conditions is brittle in character - a point of great significance explained later in this report.

BAND STRUCTURE UNDER UNIAXIAL STRAIN

The room-temperature atmospheric pressure band structure of Ge is shown in exaggerated form in figure 1.

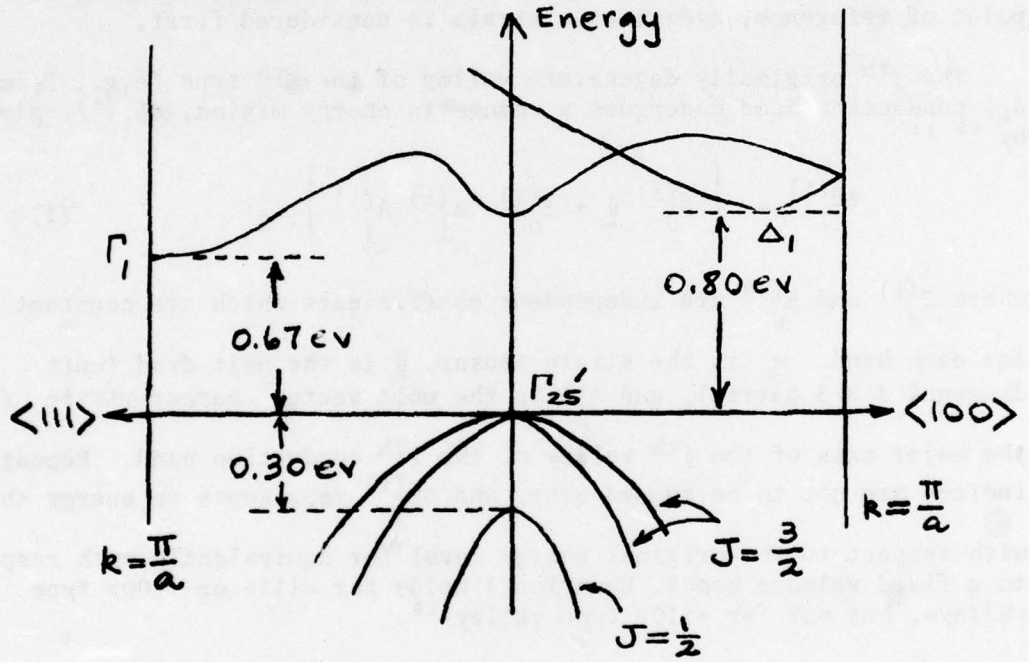

Figure 1. Room temperature - atmospheric pressure band structure of intrinsic germanium. From W. Paul and H. Brooks[9].

In room temperature-atmospheric pressure intrinsic germanium the four equivalent (<111>, <1$\bar{1}$1>, <11$\bar{1}$>, and <1$\bar{1}\bar{1}$>) Γ_1 valleys contain occupied electron states, while occupied hole states exist at the Γ_{25}' valence bands (the J = 3/2 states) near k = o.

The presence of shallow (with respect to Γ_1) donor states with the 0.67 ev gap can (and usually does) increase the number of electrons in the Γ_1 state by orders of magnitude as compared to the intrinsic case.

The variation of figure 1 with strain is calculated below. For point of reference, hydrostatic strain is considered first.

The j^{th} originally degenerate valley of the i^{th} type (e.g., Γ_1 or Δ_1) conduction band undergoes a change in energy minima, $\delta E_j^{(i)}$, given by [10] [11]

$$\delta E_j^{(i)} = \left[\Xi_d^{(i)} \underset{\sim}{\|} + \Xi_u^{(i)} \underset{\sim}{A}_j^{(i)} \underset{\sim}{A}_j^{(i)} \right] : \underset{\sim}{\varepsilon} \qquad (1)$$

where $\Xi_d^{(i)}$ and $\Xi_u^{(i)}$ are independent coefficients which are constant for each band. $\underset{\sim}{\varepsilon}$ is the strain tensor, $\underset{\sim}{\|}$ is the unit dyad (unit diagonal 3 x 3 matrix), and $\underset{\sim}{A}_j^{(i)}$ is the unit vector characteristic of the major axis of the j^{th} valley of the i^{th} conduction band. Repeated indices are not to be summed over, and $\delta E_j^{(i)}$ represents an energy shift with respect to the original energy level (or equivalently with respect to a fixed valence band). Equation 1 holds for <111> or <100> type valleys, but not for <110> type valleys[10].

Denoting <111> type valleys by the superscript 1, and <100> type valleys by the superscript 2, allows one to write

$$\underset{\sim}{A}_1^{(1)} = \frac{\hat{\varepsilon}_1}{\sqrt{3}} + \frac{\hat{\varepsilon}_2}{\sqrt{3}} + \frac{\hat{\varepsilon}_3}{\sqrt{3}} \quad , \quad \underset{\sim}{A}_2^{(1)} = \frac{\hat{\varepsilon}_1}{\sqrt{3}} - \frac{\hat{\varepsilon}_2}{\sqrt{3}} + \frac{\hat{\varepsilon}_3}{\sqrt{3}}$$

$$\underset{\sim}{A}_3^{(1)} = \frac{\hat{\varepsilon}_1}{\sqrt{3}} + \frac{\hat{\varepsilon}_2}{\sqrt{3}} - \frac{\hat{\varepsilon}_3}{\sqrt{3}} \quad , \quad \underset{\sim}{A}_4^{(1)} = \frac{\hat{\varepsilon}_1}{\sqrt{3}} - \frac{\hat{\varepsilon}_2}{\sqrt{3}} - \frac{\hat{\varepsilon}_3}{\sqrt{3}}$$

and for the six <100> type valleys (the relatively unoccupied Δ_1 band in Ge)

$$\underset{\sim}{A}_1^{(2)} = -\underset{\sim}{A}_2^{(2)} = \hat{\varepsilon}_1 \ , \quad \underset{\sim}{A}_3^{(2)} = -\underset{\sim}{A}_4^{(2)} = \hat{\varepsilon}_2 \ , \quad \underset{\sim}{A}_5^{(2)} = -\underset{\sim}{A}_6^{(2)} = \hat{\varepsilon}_3 \ ,$$

where $\hat{\varepsilon}_i$ denotes a unit vector along the i^{th} crystal cube axis (e.g. $\hat{\varepsilon}_2$ is the unit vector parallel to the <010> cube edge).

The two J = 3/2 bands which are degenerate (fig. 1) at k = o undergo a strain induced energy change,

$$\delta E_y^{(\pm)} \ , \text{ at } \underset{\sim}{k} = o \text{ given}^{11} \text{ by}$$

$$\delta E_v^{(\pm)} = a \underset{\sim}{1} : \underset{\sim}{\varepsilon} \pm \sqrt{\frac{b^2}{2}\left[(\varepsilon_{11} - \varepsilon_{22})^2 + \text{cp}\right] + d^2(\varepsilon_{xy}^2 + \text{cp})}, \qquad (2)$$

where a, b, and d are Material constants, and cp denotes cyclic permutation.

Hydrostatic Compression

In keeping with the usual shock wave convention, this report takes strain as positive in compression. Thus for hydrostatic compression,

$$\underset{\sim}{\varepsilon} = \varepsilon_o \begin{pmatrix} 100 \\ 010 \\ 001 \end{pmatrix} \qquad (3)$$

Substituting equation 3 into equations 1 and 2 gives

$$\delta E_i^{(1)} = 3\left(\Xi_d^{(1)} + \frac{\Xi_u^{(1)}}{3}\right)\varepsilon_o, \text{ all i} \qquad (4)$$

$$\delta E_i^{(2)} = 3\left(\Xi_d^{(2)} + \frac{\Xi_u^{(2)}}{3}\right)\varepsilon_o, \text{ all i} \qquad (5)$$

$$\delta E_v^{(\pm)} = 3\,a\,\varepsilon_o. \qquad (6)$$

Thus none of the originally degenerate bands split in the hydrostatic compression case (as expected, because hydrostatic compression maintains the original crystal symmetry).

Ξ_u values exist as independent data (from acoustoelectric[12] and piezoresistance[13] experiments), while Ξ_d values do not exist independently. Optical band gap transition experiments[9,11] measure

$$\left[\delta E_i^{(1,2)} - \delta E_v^{(\pm)}\right].$$

From the Paul and Brooks[9] data†

$$\left[\Xi_d^{(1)} + \frac{\Xi_u^{(1)}}{3} - a\right] = 5.0 \text{ ev}, \tag{7}$$

$$\left[\Xi_d^{(2)} + \frac{\Xi_u^{(2)}}{3} - a\right] = -1.5 \text{ ev}. \tag{8}$$

Error values have been omitted from equations 7 and 8. The effect of such experimental errors, although not important to the concepts being presented here, is treated in the analysis of <110> uniaxial strain induced energy shifts.

In this report all calculations are carried out for stress (pressure) values of 50 kb. As only essentially linear theory (see the <110> strain summary) is being considered, simple scaling yields predictions for any stress value. Employing a bulk modulus value, $K = 7.50 \times 10^{11}$ cgs, and

$$P = K\frac{\Delta V}{V_o}, \quad \frac{\Delta V}{V_o} = 3\,\epsilon_o \Rightarrow \epsilon_o = \frac{P}{3K} \tag{9}$$

gives for 50 kb

$$\epsilon_o\{50\} = 2.22 \times 10^{-2} \tag{10}$$

---

†In converting the Paul and Brooks[9] data to a strain basis a bulk modulus value of $K = 7.50 \times 10^{11}$ cgs has been used. The Paul and Brooks data are used here because it is based on room temperature, and equations 7 and 8 are known[11] to exhibit a strong temperature dependence. The Balslev[11] data are for 80 K.

Substituting equations 7-10 into equations 4-6 yields the energy level shifts illustrated in figure 2.

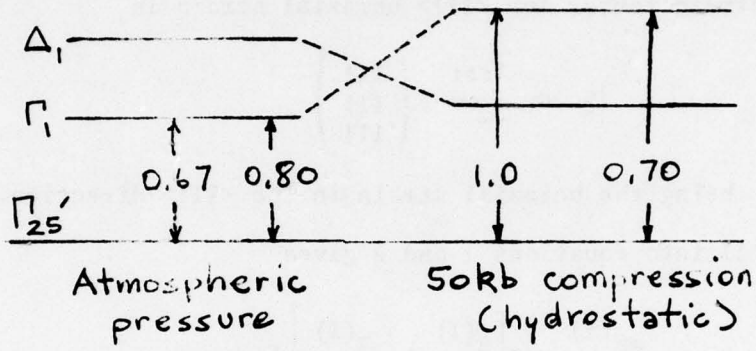

Figure 2. Energy level shifts for 50 kb hydrostatic compression. Energies are in electron volts.

The <111> and <100> band crossing at approximately 35 kb has been verified experimentally[14] (and has been well understood for many years). The <100> band is predicted to collapse into the valence band at approximately

$$\left(\frac{0.80}{0.10} \times 50\right) = 400 \text{ kb.}$$

Hydrostatic electrical resistivity (room temperature) experiments[4] show a semiconductor-to-metallic transition at approximately 115 kb.

Hydrostatic Strain Summary

The experimentally observed 115 kb hydrostatic semiconductor-metal transition is in no way correlated with any band crossings. Thus that hydrostatic transition must be associated with a polymorphic (structural) phase transition wherein the new phase has a collapsed conduction band-valence band structure. Furthermore the near room-temperature 115 kb transition is quite sluggish (ref. 4, fig. 5), casting some doubt on the ability to observe it under dynamic shock wave conditions.

The hydrostatic experiments[4, 14] do not show any evidence of the approximately 50 kb uniaxial strain transition (table 1) observed under shock wave conditions. This is a direct indication that shear (which is not present hydrostatically) is important for the 50 kb shock transition.

<111> Uniaxial Strain

The strain tensor for <111> uniaxial strain is

$$\underset{\sim}{\varepsilon} = \frac{\varepsilon_{111}}{3} \begin{pmatrix} 111 \\ 111 \\ 111 \end{pmatrix}, \tag{11}$$

with ε_{111} being the uniaxial strain in the <111> direction. Substituting equation 11 into equations 1 and 2 gives

$$\delta E^{(1)}_{<111>} = \left[\Xi^{(1)}_d + \Xi^{(1)}_u \right] \varepsilon_{111}, \tag{12}$$

$$\delta E^{(1)}_i = \left[\Xi^{(1)}_d + \frac{\Xi^{(1)}_u}{9} \right] \varepsilon_{111}, \quad i \equiv \left\{ \begin{matrix} <1\bar{1}1> \\ <11\bar{1}> \\ <1\bar{1}\bar{1}> \end{matrix} \right\}, \tag{13}$$

$$\delta E^{(2)}_i = \left[\Xi^{(2)}_d + \frac{\Xi^{(2)}_u}{3} \right] \varepsilon_{111}, \tag{14}$$

$$\delta E^{(\pm)}_v = a\, \varepsilon_{111} \pm \frac{| \varepsilon_{111} d |}{\sqrt{3}}. \tag{15}$$

The procedure now is to evaluate

$$\delta E_{av}^{(1)} \equiv \left[\left(\Xi_d^{(1)} + \frac{\Xi_u^{(1)}}{3} \right) - a \right] \varepsilon_{111} , \tag{16}$$

$$\delta E_{av}^{(2)} \equiv \left[\left(\Xi_d^{(2)} + \frac{\Xi_u^{(2)}}{3} \right) - a \right] \varepsilon_{111} , \tag{17}$$

and then to calculate the <111> strain-induced band splitting with respect to the average band motion of equation 16.

If T_{111} is the <111> directed stress, then[15]

$$T_{111} = \sigma_{11} + 2\sigma_{12} , \tag{18}$$

where σ_{ij} is the stress measured in the cube axis coordinate system. The σ_{ij} are related to the cube axis coordinate strains, and thus ε_{111} through equation 11, by[15]

$$\sigma_{11} = \left(C_{11} + 2\, C_{12} \right) \frac{\varepsilon_{111}}{3} , \quad \sigma_{12} = \frac{2}{3}\, C_{44}\, \varepsilon_{111} , \tag{19}$$

so that

$$\varepsilon_{111} = \frac{3\, T_{111}}{C_{11} + 2\, C_{12} + 4\, C_{44}} . \tag{20}$$

Employing the elastic constant values

$$C_{11} = 1.29 \times 10^{12} \text{ cgs}$$

$$C_{12} = 4.83 \times 10^{11} \text{ cgs}$$

$$C_{44} = 6.71 \times 10^{11} \text{ cgs}$$

gives an ε_{111} value corresponding to 50 kb (for T_{111}) of

$$\varepsilon_{111}\{50\} = 3.64 \times 10^{-2} . \tag{21}$$

Equations 7 and 8, along with equation 22, then suffice to determine the average band motion of equations 16 and 17.

The <111> band splitting is determined by subtracting equation 16, with a = o, from equations 12 and 13. The result is

$$\Delta E^{(1)}_{<111>} \equiv \left[\left(\Xi^{(1)}_d + \Xi^{(1)}_u \right) - \left(\Xi^{(1)}_d + \frac{\Xi^{(1)}_u}{3} \right) \right] \varepsilon_{111}$$

$$\Delta E^{(1)}_{<111>} = \frac{2}{3} \Xi^{(1)}_u \varepsilon_{111} \, . \tag{22}$$

$$\Delta E^{(1)}_{i} = - \frac{2}{9} \Xi^{(1)}_u \varepsilon_{111} \, . \tag{23}$$

The deformation potential $\Xi^{(1)}_u$ is known[16] to exhibit a temperature dependence (although apparently not as strong as that of the indirect band gap values of equations 7 and 8). In this report

$$\Xi^{(1)}_u = - 16.7 \text{ ev} \tag{24}$$

(minus sign for strain positive in compression) is used. That value is based upon piezoresistance measurements as a function of temperature by Morin, Geballe, and Herring[17], and should be fairly representative of room temperature. The 16.7 ev value is consistent with relaxation time experiments[18] and is essentially equal to the 80 K Balslev[11] value of (16.2 $\pm$ 0.4) ev.

The average band motions, when combined with equations 21-24, and the splitting component of equation 15 give the 50 kb band structure illustrated in figure 3. In arriving at figure 3, the Balslev[11] value of d = 3.7 ev has been used for the strain-induced valence band splitting. Figure 3 predicts that the conduction band collapses onto the valence band at a <111> uniaxial strain corresponding stress of

$$\left[\frac{0.67}{(0.67 - 0.37)} \times 50 \right] \text{ kb} = 112 \text{ kb.}$$

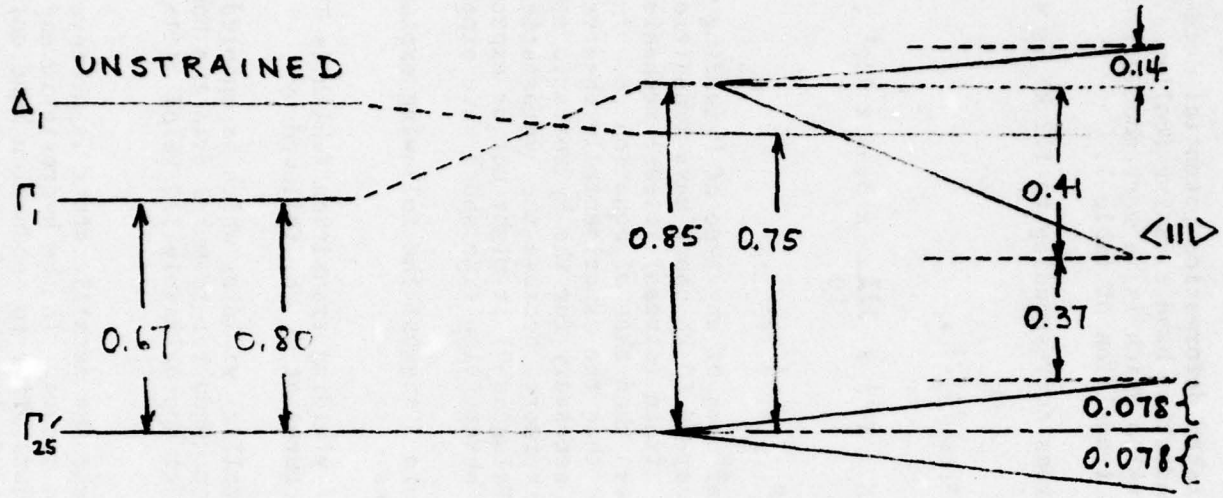

Figure 3. Energy level shifts for <111> uniaxial strain (with a corresponding stress of 50 kb) in Ge.

<111> Strain Summary

Fairly well established deformation potential data predict a valence band and <111> conduction band crossing (collapse) at approximately 112 kb - a value which is in very good agreement with the observed 125 kb shock transition of table 1.

The hydrostatic stress corresponding to 112 kb is simply given by

$$P_{112} = K\, \epsilon_{111}\, \{112\}\,, \tag{25}$$

or

$$P_{112} = 7.5 \times 10^{11} \times \frac{112}{50} \times 3.64 \times 10^{-2}\,,$$

$$\therefore P_{112} = 61 \text{ kb}. \tag{26}$$

Equation 25 neglects the effects of any type of "yielding which may be associated with the observed 50 kb shock wave transition (table 1). Such yielding serves as a strain (stress) release mechanism leading to a hydrostatic stress less than that of equation 26. In any event, 61 kb is considerably less than the experimentally observed[4, 14] hydrostatic pressure of 115 kb necessary for the hydrostatic semiconductor-to-metal transition. Furthermore, because the hydrostatically observed transition is slow (i.e. "sluggish") it might not be expected to be observable in microsecond observation time shock wave experiments.

The numbers in figure 3 suggest the following explanation for the shock wave observations:

1. Some type of yielding transition (which is TENTATIVELY identified as brittle fracture) at 50 kb, followed by

2. Ductile (metallic) yielding which is enabled by the uniaxial strain induced semiconductor-to-metal (via the band gap going to zero) transition at approximately 112 kb of <111> uniaxial equivalent strain.

In the shock wave experiment the metallic state is achieved before the polymorphic transition occurs. In the hydrostatic experiment a polymorphic transition occurs prior to conduction band collapse, and the band structure associated with the new phase is undoubtedly metallic.

The consequences of the observed 50 kb transition have been neglected in the scaling to the 120 kb region. The apparent elastic constants can undergo large changes when a mechanical transition is traversed. That neglect represents a potentially important difficulty. Because, however, plasticity does not result in a net volume change, plasticity associated with the 50 kb transition only indirectly affects the strain to be associated with the deformation potential uniaxial strain calculations. This question of elastic-plastic is considered further in the <100> uniaxial strain summary of this report (where the calculations are the least complicated). While much more work needs to be done on this elastic-plastic question, it appears that the 50 kb transition can be neglected in scaling at least to zeroth order.

<100> Uniaxial Strain

Here the strain, again referred to a cube axis coordinate system, is

$$\underset{\sim}{\varepsilon} = \varepsilon_{100} \begin{pmatrix} 100 \\ 000 \\ 000 \end{pmatrix}. \tag{27}$$

And upon again employing equations 1 and 2

$$\delta E_i^{(1)} = \left[\Xi_d^{(1)} + \frac{\Xi_u^{(1)}}{3} \right] \varepsilon_{100}, \text{ all i.} \tag{28}$$

$$\delta E_j^{(2)} = \left[\Xi_d^{(2)} + \Xi_u^{(2)} \right] \varepsilon_{100}, \; j = 1,2. \tag{29}$$

$$\delta E_k^{(2)} = \Xi_d^{(2)} \varepsilon_{100}, \; k = 3,4,5,6. \tag{30}$$

In equations 29 and 30, the j and k values refer to the individual <100> type valley minima discussed previously.

$$\delta E_v^{(\pm)} = a \varepsilon_{100} \pm |b \varepsilon_{100}| \tag{31}$$

For <100> uniaxial strain only the <100> minima and the valence band are split. The valence band splitting is given by the second term on the right of equation 31, and the <100> splitting with respect to the mean energy is given by

$$\Delta E_j^{(2)} = \frac{2}{3} \Xi_u^{(2)} \varepsilon_{100}, \; j = 1,2. \tag{32}$$

$$\Delta E_k^{(2)} = -\frac{1}{3}\,\Xi_u^{(2)}\,\varepsilon_{100}\,, \quad k = 3,4,5,6. \tag{33}$$

The value of $\Xi_u^{(2)}$ for Ge has not been determined experimentally. There does, however, appear to be great similarity between the deformation potential coefficients for Ge and Si. The hydrostatic motion of the <100> indirect band gap in Ge is equal[9] to that in Si (where the <100> minima are occupied). Thus

$$\Xi_u^{(2)} = -\,8.6 \text{ ev}, \tag{34}$$

(minus sign for strain positive in compression) is taken from Si experimental[11] values and used here. The Balslev[11] value of b = 1.8 ev is used in equation 31.

The strain ε_{100} corresponding to 50 kb is given by

$$\varepsilon_{100} = \frac{T_{100}}{c_{11}}\,, \tag{35}$$

$$\varepsilon_{100}\ \{50\} = 3.88 \times 10^{-2} \tag{36}$$

The results of completing the calculations indicated above are illustrated in figure 4.

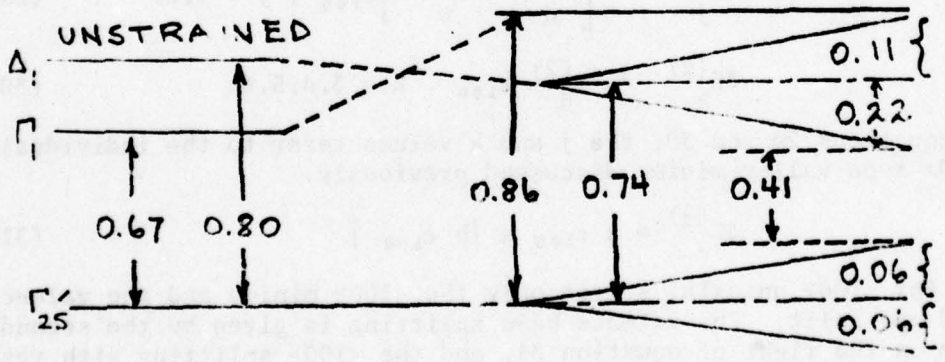

Figure 4. Energy level shifts for <100> uniaxial strain (corresponding stress of 50 kb).

<100> Strain Summary

Although the figure 4 results are slightly suspect because of the use of the $\Xi_u^{(2)}$ silicon value, these results are entirely consistent with the overall point of view being presented in this report. Two of the <100> conduction band minimas are predicted to collapse onto the upward moving split $J = 3/2$ valence band at a <100> uniaxial stress level corresponding to

$$\left[\frac{0.80}{(0.80 - 0.41)} \times 50\right] \text{kb} = 102 \text{ kb}.$$

The above 103 kb value is consistent with the table 1 experimental value of 117 kb for the <100> observed shock transition. It is also consistent with the observed ordering of the <100> and <111> shock transitions in that the numbers of this report predict a conduction band collapse for <100> uniaxial strain at a lower stress than the 112 kb prediction for the <111> uniaxial strain case. It is necessary, however, to urge caution because of the somewhat guessed value for $\Xi_u^{(2)}$.

As mentioned in the <111> uniaxial strain summary, this report neglects elastic-plastic effects associated with the 50 kb transition.

Above the 50 kb transition the total uniaxial strain has elastic and plastic components. If "e" denotes elastic and "p" plastic, then the total strain components may be written as

$$\varepsilon_{11} = \varepsilon_{11}^e + \varepsilon_{11}^p ,$$

$$\varepsilon_{\perp} = \varepsilon_{\perp}^e + \varepsilon_{\perp}^p = o \text{ (uniaxial condition)},$$

$$\varepsilon_{11}^p + 2\varepsilon_{\perp}^p = o \text{ (no plastic volume change)},$$

where 11 (parallel) denotes the (<100>, <100>) strain component. $\perp$ denotes a perpendicular (e.g. (<010>, <010>)) component.

Only the elastic strains are important for volume changes associated with the deformation potential calculations. Thus equation 27 should be replaced by

$$\underset{\sim}{\varepsilon}^{e} = \begin{pmatrix} \varepsilon_{11}^{e} & o & o \\ o & \varepsilon_{\perp}^{e} & o \\ o & o & \varepsilon_{\perp}^{e} \end{pmatrix}$$

above the 50 kb transition. $\underset{\sim}{\varepsilon}^{e}$ can be rewritten as

$$\underset{\sim}{\varepsilon}^{e} = \begin{pmatrix} \varepsilon_{\perp}^{e} & o & o \\ o & \varepsilon_{\perp}^{e} & o \\ o & o & \varepsilon_{\perp}^{e} \end{pmatrix} + \begin{pmatrix} \varepsilon_{11}^{e} - \varepsilon_{\perp}^{e} & o & o \\ o & o & o \\ o & o & o \end{pmatrix}$$

Thus the $\underset{\sim}{\varepsilon}^{e}$ for deformation potential considerations may be viewed as being composed of a hydrostatic elastic compression plus a uniaxial strain smaller than that predicted by equation 36 if $\varepsilon_{\perp}^{e}$ is positive.

As the hydrostatic and uniaxial parts of $\underset{\sim}{\varepsilon}^{e}$ are additive, the results remain virtually unchanged (other than for the effect of the $\varepsilon_{\perp}^{e}$ components). Nevertheless, elastic-plastic effects represent an important area of future work (especially in the <111> and <110> uniaxial strain geometrics).

<110> Uniaxial Strain

The cube axis referred strain is given by

$$\underset{\sim}{\varepsilon} = \frac{\varepsilon_{110}}{2} \begin{pmatrix} 110 \\ 110 \\ 000 \end{pmatrix} \qquad (37)$$

Substituting equation 37 into equations 1 and 2 gives

$$\delta E_i^{(1)} = \left[\Xi_d^{(1)} + \frac{2}{3} \Xi_u^{(1)} \right] \varepsilon_{110}, \quad i = 1,3. \tag{38}$$

$$\delta E_j^{(1)} = \Xi_d^{(1)} \varepsilon_{110}, \quad j = 1,2. \tag{39}$$

$$\delta E_i^{(2)} = \left[\Xi_d^{(2)} + \frac{\Xi_u^{(2)}}{2} \right] \varepsilon_{110}, \quad i = 1,2,3,4. \tag{40}$$

$$\delta E_j^{(2)} = \Xi_d^{(2)} \varepsilon_{110}, \quad j = 5,6, \tag{41}$$

where the i and j values refer to the specific valley minima identified earlier (following equation 2).

$$\delta E_v^{(\pm)} = a\,\varepsilon_{110} \pm \sqrt{b^2 \left(\frac{\varepsilon_{110}}{2} \right)^2 + 2d^2 \left(\frac{\varepsilon_{110}}{2} \right)^2}, \tag{42}$$

or

$$\delta E_v^{(\pm)} = a\,\varepsilon_{110} \pm \frac{\varepsilon_{110}}{2} \sqrt{b^2 + 2d^2}. \tag{43}$$

The <111> band splitting with respect to the mean is given by

$$\Delta E_i^{(1)} = \frac{1}{3} \Xi_u^{(1)} \varepsilon_{110}, \quad i = 1,3, \tag{44}$$

$$\Delta E_j^{(1)} = -\frac{1}{3} \Xi_u^{(1)} \varepsilon_{110}, \quad j = 2,4. \tag{45}$$

The <100> band splitting with respect to the mean is

$$\Delta E_i^{(2)} = \frac{1}{6} \Xi_u^{(2)} \varepsilon_{110}, \quad i = 1,2,3,4, \tag{46}$$

$$\Delta E_j^{(2)} = -\frac{1}{3} \Xi_u^{(2)} \varepsilon_{110}, \quad j = 5,6. \tag{47}$$

The uniaxial strain corresponding to the 50 kb shock wave experiment is determined[15] by

$$T_{110} = \sigma_{11} + \sigma_{12} \, , \tag{48}$$

$$\sigma_{11} = (c_{11} + c_{12}) \frac{\varepsilon_{110}}{2} \, , \; \sigma_{12} = c_{44} \, \varepsilon_{110} , \tag{49}$$

where σ_{ij} is the stress tensor measured in the cube axis coordinate system. Combining equations 48 and 49 yields

$$\varepsilon_{110} = \frac{2 \, T_{110}}{c_{11} + c_{12} + 2 \, c_{44}} \tag{50}$$

$$\therefore \varepsilon_{110} \{50\} = 3.21 \times 10^{-2} . \tag{51}$$

Combining the above <110> strain equations with the deformation potential values expressed previously results in figure 5.

<110> Strain Summary

Figure 5 predicts that

1. Two <111> type valleys will collapse onto a split-off valence band at a <110> uniaxial strain equivalent stress of

$$\left\{ \left(\frac{0.67}{0.67 - 0.56} \right) \times 50 \right\} \text{ kb} = 305 \text{ kb.}$$

2. Four <100> type valleys will collapse onto a split-off valence band at a <110> uniaxial strain equivalent stress of

$$\left\{ \left(\frac{0.80}{0.80 - 0.19} \right) \times 50 \right\} \text{ kb} = 211 \text{ kb.}$$

It is thus seen that the <110> uniaxial strain prediction is too high (211 kb vs the 125 kb experimental value of table 1). Assuming that the model proposed in this report is correct, the reason for the large <110> uniaxial strain experimental-theoretical discrepancy is not clear.

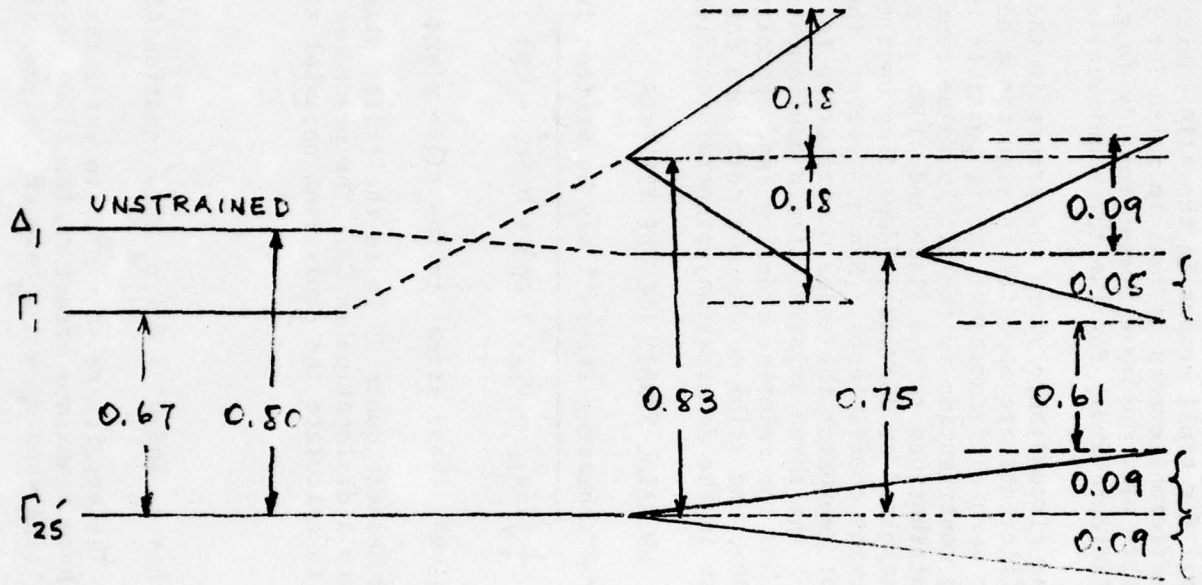

Figure 5. Energy level shifts for <110> uniaxial stress (50 kb corresponding stress).

As previously mentioned, there is some uncertainty in the various deformation potential coefficients. The theory presented here is exactly linear in the <111> and <100> uniaxial strain cases, and essentially linear† for small errors in the <110> uniaxial strain case. The effect of coefficient errors is thus to raise (or lower) the conduction band-valence band collapse stress equally (e.g. by 10% for a 10% uniform coefficient error) for the three uniaxial strain directions.

Only in the circumstance where the errors in the b and d valence band coefficients are opposite in sign can a non-uniform effect arise. In such a circumstance, it is possible to have the valence splitting contribution to the 211 kb value remain unchanged while valence contributions to the <111> and <100> strain collapse cases could be increased or decreased (depending upon the sign of the error in the relevant coefficient). Since, however, the valence band-splitting does not represent the major contribution to the energy gap closure for any of the three uniaxial strain configurations, it is difficult to see how the relative ordering (and approximate magnitudes) of our <111>, <100>, and <110> collapse predictions can be greatly affected by errors in the deformation potential coefficients.

UNIAXIAL STRAIN DUCTILE YIELDING

The "octahedral" shearing stress[19] may be written in the form

$$\tau_{oct} = \frac{1}{3}\sqrt{\{(\sigma_{11} - \sigma_{22})^2 + cp\} + b\{\sigma_{12}^2 + cp\}} \cdot \qquad (52)$$

τ_{oct} is the "resolved" shear stress in the <111> plane.

Alexander and Haasen[7] quote 25 kb as the (<111> plane) shear stress necessary to create a dislocation in Ge. The procedure is thus to set τ_{oct} = 25 kb and to calculate the equivalent uniaxial strain corresponding stress.

---

†Substitute $b' = b + \varepsilon_b$ and $d' = d + \varepsilon_d$ into equation 43, and expand the square root. The errors are then seen to enter the final result linearly, and to have a maximum effect on the <110> uniaxial strain valence band-splitting when ε_b and ε_d are of the same sign.

<100> Uniaxial Strain

Here, using equation 27, it is easily seen that

$$\sigma_{11} = c_{11}\,\varepsilon_{100}\ ,\ \sigma_{22} = \sigma_{33} = c_{12}\,\varepsilon_{100}\ , \tag{53}$$

so that

$$\tau_{oct} = \frac{\sqrt{2}}{3}\,(c_{11} - c_{12})\,\varepsilon_{100}\ , \tag{54}$$

or

$$\tau_{oct} = \frac{\sqrt{2}}{3}\left(1 - \frac{c_{12}}{c_{11}}\right)\sigma_{11}\ . \tag{55}$$

Setting τ_{oct} = 25 kb and, using the previously listed elastic constant values, gives

$$\sigma_{11} = \frac{\tau_{oct}}{0.30} = 83\ \text{kb} \tag{56}$$

<111> Uniaxial Strain

From equations 18 and 19, and†

$$\sigma_{xy} = c_{44}\,\frac{\varepsilon_{111}}{3} \tag{57}$$

it is easily seen that

$$\tau_{oct} = \frac{2}{3}^{3/2}\,c_{44}\,\varepsilon_{111} \tag{58}$$

†The factor of 2 appears in equation 57 because Chou and Pagano[15] use a shear strain twice that associated with equations 11 and 37.

and finally employing equation 20 gives

$$\tau_{oct} = \frac{2^{3/2} c_{44}}{c_{11} + 2 c_{12} + 4 c_{44}} T_{111} , \qquad (59)$$

where T_{111} is the <111> directed stress corresponding to <111> uniaxial stress.

Thus upon using the previously listed elastic constant values and τ_{oct} = 25 kb, one sees that

$$\tau_{oct} = 2^{3/2}\left(\frac{0.671}{4.94}\right) \tau_{111}, \qquad (60)$$

or

$$\tau_{111} = 2.60\ \tau_{oct} = 65 \text{ kb}. \qquad (61)$$

<110> Uniaxial Strain

From equations 37, 48, 49, and 52

$$\sigma_{11} = \sigma_{22} = (c_{11} + c_{12}) \frac{\varepsilon_{110}}{2}$$

$$\sigma_{33} = 2 c_{12} \frac{\varepsilon_{110}}{2} , \qquad (62)$$

$$\sigma_{12} = c_{44} \varepsilon_{110} ,$$

$$\sigma_{23} = \sigma_{31} = 0 ,$$

$$\tau_{oct} = \frac{\varepsilon_{110}}{3} \sqrt{\frac{(c_{11} - c_{12})^2}{2} + 6 c_{44}^2} , \qquad (63)$$

or upon using equation 50

$$T_{110} = \frac{3}{2} \frac{(c_{11} + c_{12} + 2 c_{44}) \tau_{oct}}{\sqrt{\frac{(c_{11} - c_{12})^2}{2} + 6 c_{44}^2}} \qquad (64)$$

$$\therefore \quad T_{110} = \left(\frac{3}{2}\right) \left(\frac{3.113}{1.74}\right) \tau_{oct}, \tag{65}$$

$$T_{110} = 67 \text{ kb}, \tag{66}$$

where τ_{oct} = 25 kb has **again** been used.

There are two points to be made concerning the numerical results displayed in equations 56, 61, and 66:

1. The <111> plane shear stress necessary for dislocation generation corresponds to a uniaxial strain equivalent stress at least 30% higher than the observed 50 kb first shock wave transition (table 1).

2. Equations 56, 61, and 66 are consistent with conduction band-valence band collapse being the switch which allows the lower stress (65, 67, and 83 kb) dislocation generation to proceed in a ductile medium.

CONCLUSIONS

A rough equivalency has been demonstrated between the uniaxial strain corresponding stress for conduction band-valence band collapse and the approximately 120 kb observed shock wave transition. If difficulty with the calculations exists, it is to be found in the high (211 kb) claculated stress associated with the <110> uniaxial strain case.

The TENTATIVE conclusion, based upon the observation that brittle fracture precedes ductile yielding in room temperature Ge, is that the 50 kb shock wave transition is brittle in character. That brittle fracture then is followed by a conduction band-valence band collapse at approximately 120 kb (211 kb for <110> uniaxial strain) which acts as an enabling switch for ductile (metallic) yielding.

As mentioned previously, the presence of brittle fracture at 50 kb must certainly (in that it acts as a stress relief mechanism) alter the strain matrices from those used in uniaxial strain calculations presented here. While it has been shown that the 50 kb elastic-plastic effects cancel to zeroth order, those effects represent an area where more theoretical work must be performed. It is, however, worth noting that perhaps a fundamental and important difference exists between the consequences of brittle and ductile yielding; brittle fracture can be thought of as resulting in pieces (cleaved) of the original material,

with each piece being essentially only elastically deformed. Ductile yielding should be a more extensive phenomenon allowing for the concept of a uniform, plastic-strain contribution.

To the extent that a dislocation phenomenon is involved in ductile yielding and brittle fracture (e.g. via dislocation twinning[8]) it is expected that the impurity content will affect the magnitude of the yielding stresses; dislocation velocity is known[7] to depend upon both the number density and the type of impurity. Because the character of an impurity can easily be changed by the strain induced shifting of an energy band (e.g., by going from a neutral to an ionized donor state as a conduction band minima decreases in energy) it is expected that impurity content will also play a role in the stress magnitude associated with the ductile and brittle yielding.

Perhaps the impurity phenomenon could selectively reduce the 211 kb value for the conduction band-valence band collapse under <110> uniaxial strain. Unfortunately it is not now known how to include such impurity effects in the type of calculations presented in this report.

REFERENCES

1. W.H. Gust and E.B. Royce, J. Appl. Phys. 43, 4437 (1972).
2. R.A. Graham et al, J. Phys. Chem. Solids 27, 1519 (1966).
3. G.E. Duvall and R.A. Graham, Rev. Modern Phys. 49, 523 (1977).
4. F.P. Bundy, J. Chem. Phys. 41, 3809 (1964).
5. Jacquesson et al, in Fifth Symposium on Detonation, Office of Naval Research Report ACR-184, U.S. Government Printing Office, Washington, DC (1970).
6. J.R. Patel and A.R. Chandhri, J. Appl. Phys. 34, 2788 (1963).
7. H. Alexander and P. Haasen, Solid State Phys. 22, 27 (1968).
8. H. Suzuki and K. Kamada, J. Phys. Soc. Japan 21, 571 (1966).
9. W. Paul and H. Brooks, Prog. in Semiconductors 7, 135 (1963).
10. C. Herring and E. Vogt, Phys. Rev. 101, 944 (1956).
11. I. Balslev, Phys. Rev. 143, 636 (1966).

12. G. Weinreich et al, Phys. Rev. 114, 33 (1959).

13. R.W. Keyes, Solid State Phys. 11, 149 (1960).

14. H.G. Drickamer, Solid State Phys. 17, 1 (1965). Fig. 49.

15. A.E.H. Love, The Mathematical Theory of Elasticity(Dover, NY, 1944).

16. H. Fritzsche, Phys. Rev. 115, 336 (1959).

17. F.J. Morin et al, Phys. Rev. 105, 525 (1957).

18. C. Herring and E. Vogt, Phys. Rev. 101, 944 (1956).

19. P.C. Chou and N.J. Pagano, Elasticity (Van Nostrand, Princeton, 1967).

DISTRIBUTION LIST

Department of the Army
Office, Chief of Research and Development
ATTN: Dr. J.I. Bryant
Washington, DC 20438

Vice President
Sandia Laboratories, Livermore
ATTN: G.R. Otey, 3157
R.S. Jacobson
Livermore, CA 94550

Director
Lawrence Livermore Laboratory
ATTN: Dr. W.H. Gust
Dr. Frank E. Walker
Dr. A.M. Karo
Livermore, CA 94550

Stanford Research Institute
Poulter Laboratories
ATTN: Dr. William J. Murri
Dr. D.R. Curran
Dr. R.K. Linde
Menlo Park, CA 94025

Director
Harry Diamond Laboratories
ATTN: Mr. Philip Brody
Washington, DC 20438

Sandia Corporation
ATTN: Dr. Walter Hermann
Dr. Robert Graham
Dr. D.B. Hayes
Dr. J. Gover (1935)
Dr. William Benedick
Dr. R.E. Hollenbach
Dr. L.D. Bertholf
P.O. Box 5800
Albuquerque, NM 87116

Washington State University
ATTN: Dr. George Duvall
Dr. G.R. Fowles
Dr. George Swan
Pullman, WA 99163

Commander
U.S. Naval Surface Weapons Center
Explosion Dynamics Division
ATTN: Dr. D. John Pastine
Dr. S.J. Jacobs
Dr. J. Forbes
Dr. James Goff
White Oak, MD 20910

Commander
U.S. Army Research Office
ATTN: Dr. H. Robl
Dr. J. Chandra
Dr. C. Boghosian
Dr. I. Lefkowitz
Dr. F. Schmiedeschoff
P.O. Box 12211
Research Triangle Park, NC 27709

Commander
U.S. Army Research & Standardization Group (Europe)
P.O. Box 65
FPO 09510

National Bureau of Standards
ATTN: Dr. Donald Tsai
Dr. Henry Prask
Gaithersburg, MD 20760

California Institute of Technology
ATTN: Dr. Thomas J. Ahrens
Dr. Lien G. Yang
Pasadena, CA 91109

Department of Chemistry & Chemical Engineering
ATTN: Dr. H.G. Drickamer
Urbana, IL 60436

Commander
ARRADCOM
Ballistic Research Laboratories
ATTN: Dr. Philip Howe
Dr. Donald Eccleshall
Dr. George Adams
Dr. John Powell
Dr. Jad H. Batteh
Dr. Robert F. Eichelberger
Mr. George E. Hauver
Dr. D.F. Strenzwilk
Dr. Y.K. Huang
Dr. I. May
Aberdeen Proving Ground, MD 21005

Commander
Benet Weapons Laboratory
ATTN: Dr. T.E. Davidson
Watervliet, NY 21289

University of Delaware
Department of Physics
ATTN: Prof. Ferd E. Williams
Prof. W.B. Daniels
Newark, DE 19711

Director
Defense Documentation Center
ATTN: DDC-TCA (12)
Cameron Station, Building 5
Alexandria, VA 22314

Union Carbide Corporation
Tarrytown Technical Center
ATTN: Dr. John B. Lightstone
Dr. Jaak Van Den Sype
Tarrytown, NY 10591

McDonnel Douglas Astronautics
ATTN: Dr. John Watcher
Dr. Harvey Berkowitz
5301 Bolsa Ave
Huntington Beach, CA 92647

Systems, Science, and Software
ATTN: Dr. H.E. Read
P.O. Box 1620
La Jolla, CA 92037

Director
Defense Nuclear Agency
ATTN: SPAS, Mr. J.F. Moulton, Jr.
Washington, DC 20305

Army Materials & Mechanics Center
ATTN: Mr. John F. Dignam
Mr. John Mescall
Dr. D.P. Dandekar
Building 131
Arsenal Street
Watertown, MA 02172

Lockheed Palo Alto Research Labs
ATTN: Dr. J.F. Riley
3251 Hanover Street
Palo Alto, CA 94304

Bell Telephone Laboratories
ATTN: Dr. A. Jayaraman, Id 230
Murray Hill, NJ 07974

Director
Los Alamos Scientific Laboratory
ATTN: Dr. J.M. Walsh
Los Alamos, NM 87544

Commander
U.S. Army Missile Research & Development Command
ATTN: Dr. Charles M. Bowden
Redstone Arsenal, AL 35809

North Carolina State University
ATTN: Prof. Y.B. Horie
Dept of Engineering Science & Mechanics
Raleigh, NC 27607

University of Tennessee
ATTN: Prof. M.A. Breazeale
Dept of Physics and Astronomy
Knoxville, TN 37916

Director
National Bureau of Standards
ATTN: Dr. V. Arp, Cryogenics Division
Boulder, CO 80302

Princeton University
ATTN: Prof. A.C. Eringen
Prof. Peter Mark
Princeton, NJ 08540

Carnegie Mellon Institute of Technology
ATTN: Prof. Morton E. Gurtin
Dr. Bernard D. Coleman
Dept. of Mathematics
Pittsburgh, PA 15213

Brown University
ATTN: Prof. Robert T. Beyer
Dept. of Physics
Providence, RI 02912

Courant Institute of Mathematical Sciences
ATTN: Library
New York University
New York, NY 10453

City College of the City University of New York
ATTN: Prof. Harry Soodak
Dept of Physics
139th Street & Convent Ave
New York, NY 10031

Queens College of the City University of New York
ATTN: Prof. Arthur Paskin
Dept of Physics
Flushing, NY 11300

SPIRE Corp
ATTN: Dr. Roger Little
Patriots Park
Bedford, MA 01730

Commander
U.S. Army ARRADCOM
ATTN: DRDAR-TD, Dr. R.E. Weigle
DRDAR-LC, Dr. J. Frasier
DRDAR-TSS (5)
DRDAR-LCN, COL Hyatt
DRDAR-LCA, Mr. W. Benson
DRDAR-LCE, Dr. R. Walker
DRDAR-LCA, Dr. Harry Fair
DRDAR-LCE, Mr. Louis Avrami
DRDAR-LCA, Dr. T. Gora
DRDAR-LCE, Dr. F. Owens
DRDAR-LCE, Dr. D. Wiegand
DRDAR-LCE, Dr. C. Capellos
DRDAR-LCE, Dr. J. Sharma
DRDAR-LCN, Dr. P. Harris (25)
DRDAR-LCN-F, Mr. A. Garcia
DRDAR-LCA, Mr. W. Doremus
DRDAR-LCA, Dr. G. Vezzolli
Dover, NJ 07801

Weapon System Concept Team/CSL
ATTN: DRDAR-ACW
Aberdeen Proving Ground, MD 21010

Technical Library
ATTN: DRDAR-CLJ-L
Aberdeen Proving Ground, MD 21010

Technical Library
ATTN: DRDAR-TSB-S
Aberdeen Proving Ground, MD 21005

Benet Weapons Laboratory
Technical Library
ATTN: DRDAR-LCB-TL
Watervliet, NY 12189

Commander
U.S. Army Armament Materiel Readiness Command
ATTN: DRSAR-LEP-L
Rock Island, IL 61299

Director
U.S. Army TRADOC Systems Analysis Activity
ATTN: ATAA-SL (Tech Lib)
White Sands Missile Range, NM 88002

U.S. Army Materiel Systems Analysis Activity
ATTN: DRXSY-MP
Aberdeen Proving Ground, MD 21005